Geochimica et Cosmochimica Acta 362 (2023) 104–114

Contents lists available at ScienceDirect

Geochimica et Cosmochimica Acta

journal homepage: www.elsevier.com/locate/gca

Hg isotope evidence for oceanic oxygenation during the Cambrian Explosion

Haifeng Fan [a,f,*], Xuewu Fu [b,f], Ruofei Yang [a,f], Hanjie Wen [c,f], Chunlin Hu [d], Jack F. Ward [e], Hongjie Zhang [a,f], Hui Zhang [b,f], Xingliang Zhang [g]

[a] State Key Lab of Ore Deposit Geochemistry, Institute of Geochemistry, CAS, Guiyang 550081, China
[b] State Key Lab of Environment Geochemistry, Institute of Geochemistry, CAS, Guiyang 550081, China
[c] School of Earth Sciences and Resources, Chang'an University, Xi'an 710054, China
[d] State Key Laboratory of Palaeobiology and Stratigraphy, Nanjing Institute of Geology and Palaeontology, CAS, Nanjing 210008, China
[e] School of the Environment, University of Queensland, Brisbane, Queensland 4072, Australia
[f] University of Chinese Academy of Sciences, Beijing 100049, China
[g] State Key Laboratory of Continental Dynamics, Shaanxi Key Laboratory of Early Life and Environments, Department of Geology, Northwest University, Xi'an 710069, China

ARTICLE INFO

Associate editor: Brian Kendall

Keywords:
Cambrian explosion
Hg isotope
Increased oxygen levels

ABSTRACT

The Cambrian explosion is a critical evolutionary milestone in life history, but the mechanistic relationship between the Cambrian explosion, rising atmospheric and oceanic oxygen levels, and the primary productivity remains controversial. Here, we present new mercury (Hg) isotope data from Cambrian marine sediments of the ~521–514 Ma Yu'anshan and Shuijingtuo Formations (Nanhua Basin, South China), which preserve the famous ~518 Ma Chengjiang and Qingjiang Cambrian Biotas, respectively. We find evidence that, prior to Cambrian animal diversification, local terrestrial and/or atmospheric inputs are important drivers of Hg enrichment in the shallow shelf Yu'anshan and Shuijintuo Formations. Elevated Hg and total organic carbon (TOC) concentrations of coeval deeper shelf and slope sections of the Niutitang Formation are mainly attributed to upwelling of Hg associated with dissolved organic carbon (Hg-DOC) from pelagic seawater, unrelated to locally high primary productivity. During the deposition of fossiliferous strata, negative shifts of Δ^{199}Hg and δ^{202}Hg values in the shallow water shelf shales from the Shuijingtuo Formation, combined with similar Hg isotope characteristics in the deeper shelf and slope shales, demonstrate a significant shallow and deep-water oxygenation event took place in the Nanhua Basin. A comparable negative shift of Δ^{199}Hg values occurs in coeval Indian Craton sediments, suggesting this oxygenation event could be regional, or possibly even global, in scale. Our newly-collected Hg isotope data provide strong evidence that rising molecular oxygen levels in both surface and deep seawater are associated with enhanced marine primary productivity and could be a critical driver of the Cambrian explosion. Finally, we also argue that Hg isotopes are an emerging and promising redox proxy for studies of Precambrian seawater, but the chemical response of Hg to atmospheric and ocean oxygenation requires further calibration.

1. Introduction

The Cambrian explosion, the rapid diversification of animal body plans and rise of ecosystem complexity across the Ediacaran–Cambrian transition, is arguably the most important evolutionary event in the history of Earth (Erwin et al., 2011). Despite its significance, however, the triggers of the Cambrian explosion remain controversial. For example, substantial increases of oceanic and atmospheric oxygen levels have been suggested to drive extraordinary ecological expansion during Cambrian time (Cloud, 1968; Knoll and Carroll, 1999; Li et al., 2017). Other studies, however, have de-emphasized the role of rising oxygen levels (Sperling et al., 2015), instead linking the Cambrian explosion to ecological, developmental, or evolutionary mechanisms under hypoxic conditions (Erwin et al., 2011; Hammarlund et al., 2018; Mills and Canfield, 2014; Sperling et al., 2013). Furthermore, Sperling and Stockey (2018), based on a comprehensive shale total organic carbon (TOC) data set, highlighted the importance of food supply for biotic radiation, suggesting that a congruent rise of primary productivity and

* Corresponding author at: State Key Lab of Ore Deposit Geochemistry, Institute of Geochemistry, CAS, Guiyang 550081, China.
E-mail address: fanhaifeng@mail.gyig.ac.cn (H. Fan).

https://doi.org/10.1016/j.gca.2023.10.020
Received 9 April 2023; Accepted 12 October 2023
Available online 14 October 2023

oxygen levels facilitated the Neoproterozoic–Cambrian increase in animal size and diversity.

The Chengjiang and Qingjiang Biotas from South China, and the Sirius Passet Biota from Greenland, represent three well-known Burgess Shale-type Biotas of Cambrian Stage 3 age (~521–514 Ma; Fu et al., 2019a; Hammarlund et al., 2019; Saleh et al., 2022), when the Cambrian explosion reached its summit (Paterson John et al., 2019; Zhang and Shu, 2021). These biotas are important archives for understanding the Cambrian explosion and associated ecosystem development, but the paleoenvironmental conditions in which they occurred are unclear. Fe speciation, $\delta^{15}N$, and trace element systematics suggest the strata-hosted Chengjiang and Sirius Passet Biotas may have been deposited in an oxygen minimum zone (Hammarlund et al., 2017; Hammarlund et al., 2019). A recent study, however, suggested that the Chengjiang fauna lived in an oxygen-rich delta front environment (Saleh et al., 2022). For the Qingjiang Biota, N isotopes have been interpreted to reflect paleoenvironmental water column chemistry like that of Chengjiang Biota (Chang et al., 2022). It is also noteworthy that organic-rich shales (TOC up to 20 wt%) are widespread in the Nanhua Basin below the Chengjiang and Qingjiang fossiliferous layers, and these have been interpreted as consequences of local high primary productivity during early Cambrian time (Cheng et al., 2020; Jin et al., 2016). However, very low quantities of TOC (<2 wt%) are observed in sedimentary rocks containing the Chengjiang, Qingjiang, and Sirius Passet fossils (Hammarlund et al., 2017; Hammarlund et al., 2019; Qi et al., 2018). It remains uncertain, therefore, whether decreasing TOC concentrations reflect a transition from a food-rich to a food-limited period or, alternatively, lower TOC due to local oxygenation.

In marine sediments, mercury (Hg) is mainly derived from atmospheric precipitation (sometimes with significant terrestrial input in nearshore environments), but extreme Hg enrichment is mostly associated with volcanism (Fitzgerald et al., 2007; Grasby et al., 2017; Grasby et al., 2019). These endmember sources are characterized by different mass-dependent and mass-independent fractionation signals (MDF and MIF, respectively; Blum et al., 2014; Sun et al., 2019). Atmospheric Hg (II) commonly shows positive MIF and negative MDF signals ($\Delta^{199}Hg = 0.39 \pm 0.28$ ‰; $\Delta^{200}Hg = 0.17 \pm 0.08$ ‰; $\delta^{202}Hg = -0.41 \pm 0.48$ ‰), unlike Hg (0) ($\Delta^{199}Hg = -0.11 \pm 0.12$ ‰; $\Delta^{200}Hg = -0.04 \pm 0.05$ ‰; $\delta^{202}Hg = 0.1 \pm 0.56$ ‰; Sun et al., 2019). Published data demonstrate that modern marine sediments dominated by atmospheric Hg usually exhibit more positive MIF signals ($\Delta^{199}Hg = 0.12 \pm 0.05$ ‰; $\Delta^{200}Hg = 0.04 \pm 0.04$ ‰) than sediments with abundant volcanic ($\Delta^{199}Hg = 0$‰; $\Delta^{200}Hg = 0$‰) and terrestrial Hg contributions ($\Delta^{199}Hg = -0.25 \pm 0.14$ ‰; $\Delta^{200}Hg = 0.02 \pm 0.04$ ‰), but MDF does not show obvious systematic variation (Blum et al., 2014; Sun et al., 2019; Zheng et al., 2018). $\Delta^{200}Hg$ variation is limited to photochemical transformations of Hg in the tropopause or stratosphere, while $\Delta^{199}Hg$ variation is caused by photochemical transformations in the troposphere and in surface waters (Blum et al., 2014). Moreover, recent studies have suggested photochemical reduction of Hg (II) is redox sensitive, and opposite $\Delta^{199}Hg$ fractionation trends occur in anoxic and oxic conditions (Bergquist and Blum, 2007; Motta et al., 2020; Zheng and Hintelmann, 2010).

In light of this sensitivity to environmental chemical conditions, Hg concentrations and isotopes in marine sediments have been used to trace volcanic emissions (e.g., (Grasby et al., 2019 and references therein) and, recently, global Ediacaran oceanic carbon cycling (Fan et al., 2021), late Archean atmospheric chemistry (Zerkle et al., 2020), and the end-Archean "whiff" of oxygen (Meixnerová et al., 2021). During the end-Archean (~2.5 Ga) "whiff" of oxygen, the oxygenated interval shows strong Hg enrichment coupled with slightly negative $\Delta^{199}Hg$ values, suggestive of increased oxidative weathering (Meixnerová et al., 2021). A strong negative shift of $\Delta^{199}Hg$ (from 0 ‰ to −0.12 ‰) recorded in deglacial banded iron formation could be associated with the oceanic oxygenation during the end of the Sturtian glaciation (Sun et al., 2022). Therefore, Hg isotopes, especially MIF, could potentially be utilized to trace atmospheric and oceanic oxygenation events, but the chemical response of Hg to atmospheric and oceanic oxygenation requires further investigation.

Here, we present Hg data from two Nanhua Basin drill cores that contain Chengjiang and Qingjiang Biota fossils. In this contribution, we first estimate the utility of Hg isotopes as a potential redox proxy by distinguishing Hg sources of the Nanhua Basin sediments, and comparing these Hg data to Mn concentrations and TOC/P (mol/mol) ratios (which are strongly controlled by benthic redox conditions; Algeo and Ingall, 2007). We then evaluate correlations between oceanic/atmospheric redox conditions and the Cambrian Explosion.

2. Geological setting

During the Cambrian Series 2 and Stage 3 (~526–514 Ma), organic-rich marine shales were deposited widely across shelf to slope and basin locations in the Nanhua Basin (Fig. 1A). The shallow shelf shales comprise the Yu'anshan Formation in Yunnan province and the Shuijintuo Formation in Hubei province (Fig. 1A). The Yu'anshan and Shuijintuo Formations host the Chengjiang and Qingjiang Biotas, respectively (Zhu et al., 2001; Fu et al., 2019a). The Chengjiang and Qingjiang Biotas are separated by ~1050 km and contain different fossil assemblages, representing communities developed in response to local environmental conditions (Fu et al., 2019a). The Qingjiang Biota is equivalent to the Chengjiang Biota in age (~518 Ma; Yang et al., 2018), and both correlate with the global Cambrian Series 2 and Stage 3 (Fu et al., 2019a). The Qingjiang Biota, however, is preserved in a somewhat more distal setting than that of the Chengjiang Biota (Fu et al., 2019a; Saleh et al., 2022).

Our Chengjiang Biota samples were collected from drill cores ZK-2808 (hereafter named Chengjiang core) in the Kunyang area from Yunnan Province. Qingjiang Biota samples were collected from drill core ZK-03 (hereafter named Qingjiang core) in the Yichang area from Hubei Province (Fig. 1A). The Chengjiang core mainly contains three members of the Yu'anshan Formation (Fig. 1B). Member I, representing sea level highstand, is composed of carbonaceous black shale. Member II is a succession of mudstones intercalated with sandstones that transitions upwards into shallower, wave-influenced fluid mud deposits. Member III, a sandstone-dominated upper member, was deposited in a storm wave-influenced shelf or distal shoreface setting (Saleh et al., 2022; Zhu et al., 2001). The ~518 Ma Chengjiang Biota (e.g., Yang et al., 2018) occurs within storm-flood-dominated delta sediments of Member II (Saleh et al., 2022; Zhu et al., 2001) (Fig. 1B), which is the thickest and most lithologically complex member of the Yu'anshan Formation. Our samples, including shales and mudstones, were only collected from Members I and II.

The Qingjiang core mainly contains three members of the Shuijingtuo Formation (Fig. 1B). Member I consists of a laminated carbonaceous black shale deposited during sea level highstand and contains an ~521 ± 5 Ma Ni-Mo sulfide layer (at 355.89 m) that correlates with Ni-Mo layers from Guizhou and Hunan provinces (Xu et al., 2011). The Qingjiang Biota is preserved in Member II, which is a black calcareous shale with subordinate sandstone deposited below storm wave base (Fu et al., 2019a). Member III is a black, centimeter–decimeter bedded limestone with thin mudstone partings, indicating a shallow water environment (Fu et al., 2019a). Our samples, including shales and mudstones, were collected from all three members of the Shuijingtuo Formation.

We also compared our investigated cores to existing Hg data from three sections of organic-rich shales belonging to the contemporaneous Niutitang Formation: the shelf Zhijin section, the slope Tongren section, and the slope Jishou section (Fig. 1A). The three sections have been well investigated in previous studies, where the Niutitang Formation is underlain by phosphorites of the Gezhongwu Formation in the Zhijin section and by cherts of the Liuchapo Formation in the Tongren and Jishou sections (Wang et al., 2020; Yin et al., 2017; Zhu et al., 2021a). Among them, slope sections show extreme enrichment of organic

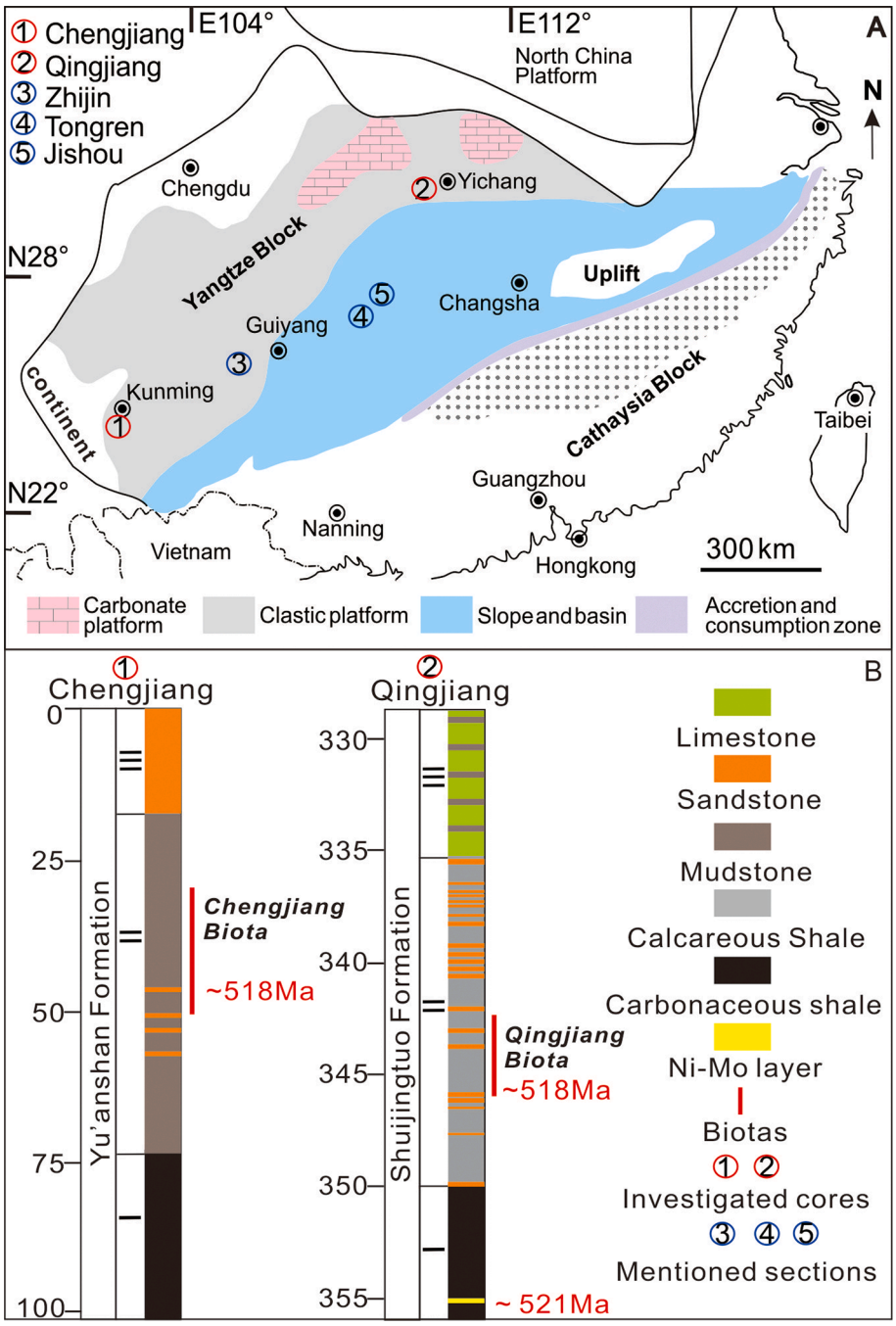

Fig. 1. A. Early Cambrian geographic map of South China (Fu et al., 2019a) showing the locations of investigated two shallow water cores (Chengjiang and Qingjiang), as well as the deeper shelf Zhijin (Yin et al., 2017), slope Tongren (Zhu et al., 2021a), and Jishou sections (Wang et al., 2020) discussed in this study. B. Simplified litho-, bio- and chrono-stratigraphy of investigated cores.

materials (mostly > 10 wt%) compared to the shelf sections (mostly < 4 wt%).

3. Methods

3.1. Hg concentrations and isotope compositions

A DMA-80 automatic Hg analyzer at the State Key Laboratory of Environmental Geochemistry, Chinese Academy of Sciences (CAS), was used to measure Hg concentrations. NIST SRM 2711a, procedural blanks, and sample duplicates were analyzed to monitor accuracy and precision. Duplicate analysis of Hg concentrations, overall, shows a small relative standard deviation (mean = ±5.5%). In this study, the mean of the duplicate tests is presented as the total Hg value.

The double-stage combustion method of Sun et al. (2013) was used to preconcentrate Hg from individual samples into 7 mL of 40 % mixed acid solution (v/v, HNO_3/HCl = 2:1). The trapping bottle and impinger were rinsed three times with 10 mL of Milli-Q water immediately after preconcentration. The Milli-Q water was added into the trapping solution, yielding a final acid concentration of ~20 %. The final trapping solutions were stored at 2–4 °C until the Hg isotope analysis was performed. A Nu Instruments cold vapor multi-collector inductively coupled plasma mass spectrometer (CV-MC-ICPMS) was used to collect Hg isotope ratios at the State Key Laboratory of Environmental Geochemistry, CAS, following the method of Fu et al. (2019b).

Standard-sample-standard bracketing using the National Institute of

Standards and Technology (NIST) Standard Reference Material (SRM) 3133 was performed to correct Hg isotope mass bias. Hg isotopic MDF are reported as delta values (δ) in per-mil (‰) relative to the mean ratios measured for the NIST SRM 3133 before and after each sample. MIF is reported in capital delta values (Δ), $\Delta^{x}Hg$ (‰) = $\delta^{x}Hg_{sample} - \beta \times \delta^{202}Hg_{sample}$, where x refers to the mass of Hg isotope (^{199}Hg, ^{200}Hg, ^{201}Hg, and ^{204}Hg). The corresponding β values of these Hg isotopes are 0.252, 0.502, 0.752, and 1.493, respectively.

Repeated analysis of NIST SRM 8610 (n = 17) and NIST SRM 2711a (Montana soil, n = 6) was performed to monitor analytical uncertainties of Hg isotopic compositions. The 2SD of these two standard references with $\delta^{202}Hg$ and $\Delta^{199}Hg$ of respectively 0.07–0.10 ‰ and 0.05–0.06 ‰ represent the typical analytical uncertainties of our samples. The measured Hg isotopic compositions of NIST SRM 8610 ($\delta^{202}Hg = -0.51 \pm 0.07$ ‰ and $\Delta^{199}Hg = -0.02 \pm 0.05$ ‰) and NIST SRM 2711a ($\delta^{202}Hg = -0.18 \pm 0.10$ ‰ and $\Delta^{199}Hg = -0.23 \pm 0.06$ ‰) agree with previously published results and are presented in Table S1.

3.2. Other elements

To measure TOC content, samples were firstly leached in 2 N HCl to remove carbonate components. Ultrapure water (18.2 MΩ-cm) was then used to rinse the leached residue three times, and the rinsed residue (representing the TOC component) was analyzed for total carbon. TOC and total sulfur (TS) contents from the Qingjiang core samples were determined using a LECO C-S Elemental Analyzer at the Institute of Geochemistry, CAS. A Flash EA 2000 Elemental Analyzer at Nanjing Institute of Geology and Palaeontology, CAS (NIGPAS) was used to analyze samples from the Chengjiang core. Manganese and phosphorous concentrations were measured via X-ray fluorescence at the ALS Chemex facility in Guangzhou, China, and an Agilent 710 ICP-OES at NIGPAS. The relative standard deviations (RSD) for these elements were better than ±5 %, based on the results of one standard reference shale (marine shale, SBC-1; Fan et al., 2021).

4. Results

4.1. Chengjiang core preserving the Chengjiang Biota

At the bottom of the Chengjiang core, from 101 m to 72 m depth, total Hg concentrations range from 111 to 190 ppb and Hg/TOC (ppb/%) varies from 64 to 112 (Fig. 2A). These samples show a narrow range

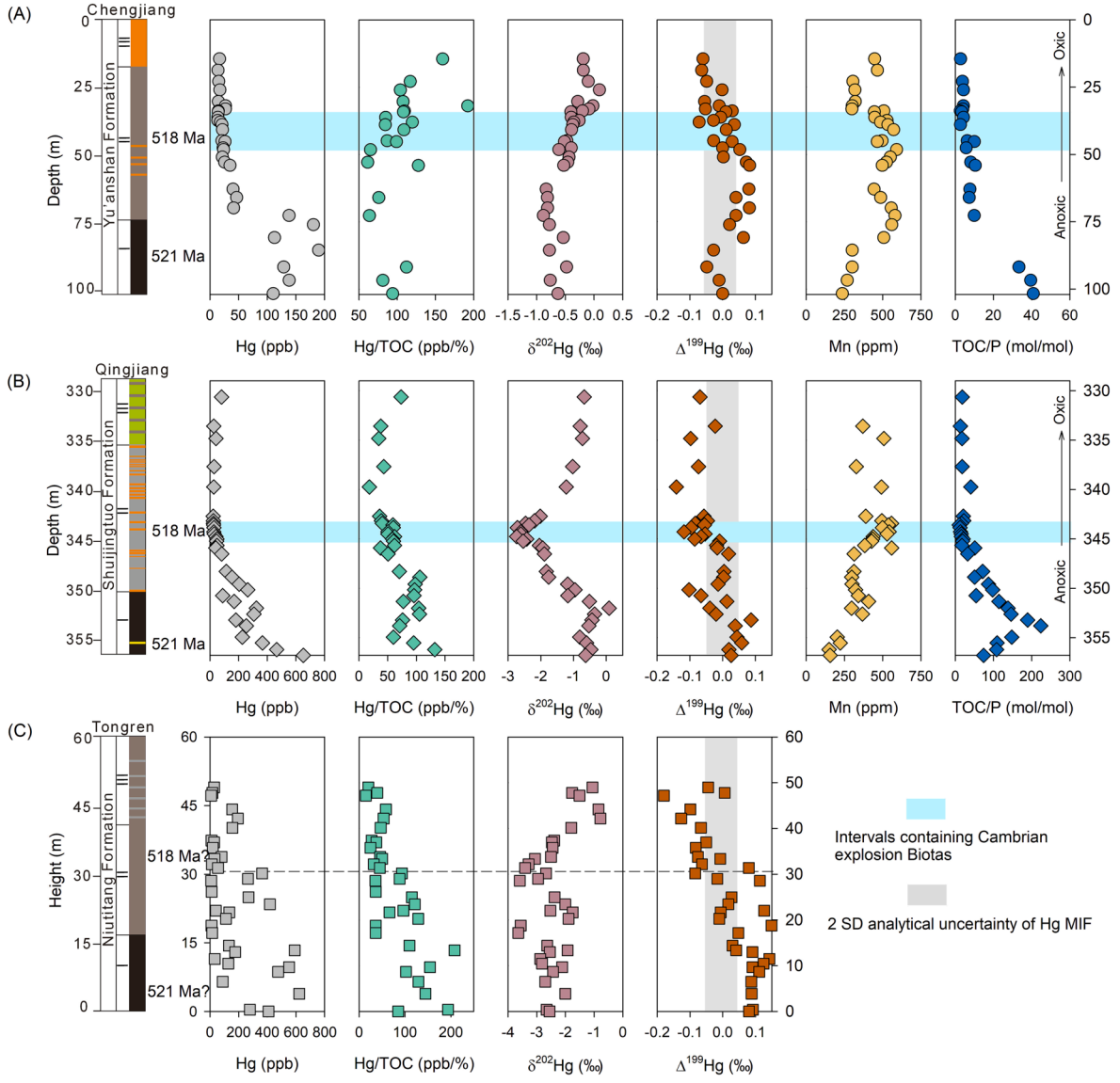

Fig. 2. Hg concentrations and isotope compositions, Hg/TOC, Mn, and TOC/P chemostratigraphy of the two newly-analyzed cores (A, Chengjiang; B, Qingjiang) and another previous published section (C, Tongren, Zhu et al., 2021a) covering ~521–514 Ma. The legends of stratigraphic column can be found in Fig. 1.

of δ^{202}Hg and Δ^{199}Hg, from −0.88 ‰ to −0.48 ‰ (−0.69 ± 0.15 ‰, mean ± 1σ standard deviation) and −0.03 ‰ to 0.06 ‰ (0.01 ± 0.04 ‰), respectively (Fig. 2A). Up section, from a depth of 70 m, total Hg gradually declines from 47 ppb to 14 ppb through the fossiliferous layer (shaded blue in Fig. 2A). Hg/TOC does change considerably due to varied TOC content upwards. δ^{202}Hg values increase from −0.81 ‰ to 0.10 ‰, and Δ^{199}Hg values decrease from 0.08 ‰ to −0.06 ‰. Throughout the whole section, Mn concentrations increase from 236 ppm to 672 ppm, and then decline to 299 ppm. TOC/P ratios gradually decrease from 41 (in the lowermost part of the core) to 3 (in the uppermost part of the core) (Fig. 2A). All data are listed in Table S2.

4.2. Qingjiang core preserving the Qingjiang Biota

In the Qingjiang core, total Hg concentrations gradually decrease from 650 ppb at the lowest part of the drill core to 40 ppb in the Qingjiang fossiliferous layers (shaded blue in Fig. 2B), and then to 20 ± 16 ppb at 343–330 m depth (Fig. 2B). Like total Hg concentrations, Hg/TOC decreases from ~150 at a depth of ~360 m depth to ~40 at ~343 m depth. In the Qingjiang core, Hg/TOC is lowest at ~339 m, where it reaches ~30, and Hg/TOC increases above this stratigraphic height. δ^{202}Hg values show relatively homogenous values (−0.53 ± 0.14 ‰) in the lowest part of the Qingjiang core (357–351 m), and they gradually decline to the lowest recorded values in the Qingjiang fossiliferous layer (−2.74 ± 0.20 ‰), before increasing above the fossiliferous layer to approximately −0.67 ‰ (Fig. 2B). The Qingjiang core Δ^{199}Hg trend is less clear, but, overall, these values decrease from slightly positive to negative values up section (Fig. 2B). Mn concentrations increase up section from 150 ppm to 558 ppm or higher values (Fig. 2B). TOC/P ratios increase from 74 to 224 in the lowermost three meters of core, before gradually decreasing from 190 to ~14. All data are listed in Table S3.

5. Discussion

5.1. Widespread Hg enrichment in the Nanhua Basin (~521 Ma)

In the Nanhua Basin, Hg enrichment comparable to that occurring in the lowest part of the Yu'anshan (Chengjiang core) and Shuijingtuo (Qingjiang core) Formations (i.e., below the fossiliferous layers; Fig. 2A and B) has been reported in deeper shelf and slope sections (Zhijin, Tongren, and Jishou sections) of the equivalent Niutitang Formation elsewhere in this Basin (Figs. 2C and 3; Wang et al., 2020; Wu et al., 2022; Yin et al., 2017; Zhu et al., 2021a,b). At that time, seawater redox conditions in the shallow shelf Chengjiang and Qingjiang settings (as well as the deeper shelf and slope locations) were oxygen-depleted or anoxic/euxinic, as demonstrated by our high TOC/P ratios (modern anoxic facies have TOC/P of ~110–200; Algeo and Ingall, 2007), low Mn concentrations (<400 ppm; Fig. 2A and B), and previous Fe speciation data (Li et al., 2017; Li et al., 2021; Wei et al., 2021). Hg enrichment in marine sediments is tightly correlated with degree of sequestration of Hg by organic materials (Grasby et al., 2019) and Hg-sulfide in strongly anoxic conditions (Shen et al., 2020; Zheng et al., 2018). The clear positive correlations of total Hg with TOC and/or TS concentrations (Fig. 3), respectively, in the two investigated cores and other referenced slope sections indicate that dissolved Hg was mainly sequestered by organic materials and/or Hg-sulfide from an anoxic seawater column prior to the Cambrian explosion. However, the mean of published Hg concentrations in marine sediments is 62 ppb (Hg/TOC ~75; Grasby et al., 2019), which is significantly less than the Hg concentrations (~100–1000 ppb, Hg/TOC mostly > 70) of the sections discussed here. Sedimentation rates and local redox conditions have been suggested to affect Hg-enrichment in sediments (Mazrui et al., 2016; Selin, 2009). However, the estimated deposition rates during this time are surprisingly similar to those found in modern euxinic basins (Lehmann et al., 2007). Additional Hg sources are, therefore, required to explain the elevated Hg concentrations in the Nanhua Basin samples (Wang et al., 2020; Wu et al., 2022; Zhu et al., 2021a). Significant additional Hg sources in the Cambrian Nanhua Basin could possibly include local terrestrial, volcanic, and pelagic (open ocean) seawater inputs. Lower Cambrian strata were deposited before the evolution of land plants (Lenton Timothy et al., 2016), and thus it is reasonable to assume that terrestrial Hg may be characterized by detrital near-zero Δ^{199}Hg and δ^{202}Hg values of −0.1 ‰ to −0.6 ‰ (i.e., similar to the composition of silicate rocks; Fan et al., 2021; Smith et al., 2008). The lower Chengjiang core sediments were deposited in a low oxygen, low energy, hemipelagic environment sometimes affected by higher-energy tractive events (Saleh et al., 2022). The relatively homogenous Δ^{199}Hg (0.01 ± 0.04 ‰) and δ^{202}Hg values (−0.69 ± 0.15 ‰) in the lowermost Chengjiang core (below 51 m depth; Fig. 2A) and Qingjiang cores (0.04 ± 0.04 ‰ and −0.55 ± 0.15 ‰, respectively, below 352 m depth; Fig. 2B) are highly consistent with that reported for pre-anthropogenic marine sediments (Δ^{199}Hg = 0.05 ± 0.01 ‰; δ^{202}Hg = −0.76 ± 0.16 ‰; Gehrke et al., 2009), which may therefore indicate that Hg enrichment is mainly attributed to local atmospheric, and possibly terrestrial Hg contributions, given higher TS concentrations at that time.

By contrast, recent studies have proposed large Hg contributions to the Nanhua Basin by volcanic activity (Wang et al., 2020; Wu et al., 2022; Zhu et al., 2021a). Most organic-rich shales in the Yu'anshan (Chengjiang core), Shuijingtuo (Qingjiang core), and Niutitang (Zhijin, Tongren and Jishou sections) Formations, however, show low–moderate Hg/TOC (ppb/%) ratios (mostly < 150) and Hg/TS (ppb/%) ratios

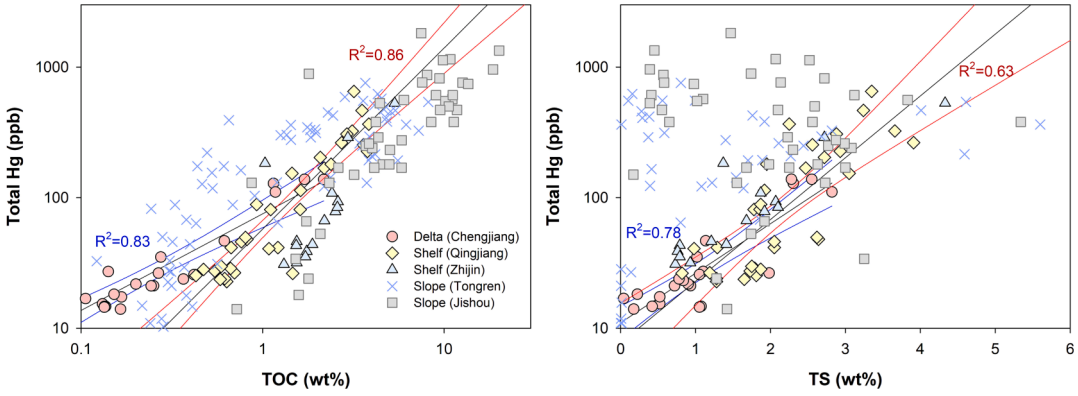

Fig. 3. Total Hg concentrations plotted against total organic carbon (TOC, A) and total sulfur concentrations (TS, B) of organic-rich shales from the Nanhua Basin. All blue lines for Chengjiang samples and all red lines for Qingjiang samples. For all samples, total Hg positively correlates with TOC, but total Hg does not positively correlate with total sulfur in most slope shales. (For interpretation of the references to colour in this figure legend, the reader is referred to the web version of this article.)

(mostly < 100, for samples with obvious correlation between Hg and TS), which are (1) much less than those of sedimentary rocks containing abundant volcanic material (Hg/TOC > 200; Grasby et al., 2019), and (2) similar to the Ordovician/Silurian marine black shales (Hg/TS less than ~300) without volcanic Hg input (Shen et al., 2019). Nevertheless, the extremely high Hg/TOC (~140–760) recorded by some Niutitang Formation slope sections has been attributed to volcanic contributions (Wang et al., 2020; Zhu et al., 2021b). Volcanic activity also commonly causes transient and extreme Hg enrichment spikes in ancient stratigraphic records (Grasby et al., 2019). Assuming that volcanic Hg was an overwhelming source for Hg enrichment in the Nanhua Basin, the homogenous δ^{202}Hg and near zero Δ^{199}Hg values could be preserved in those offshore anoxic organic-rich shales (Grasby et al., 2017). However, an obvious depth-gradient of Hg isotopes is observed in the Nanhua Basin (Figs. 3 and 4), where shallow water sediments in our investigated Chengjiang and Qingjiang cores commonly show terrestrial-like δ^{202}Hg and Δ^{199}Hg signals, compared to deeper shelf and slope sediments (δ^{202}Hg < −1.3‰; Δ^{199}Hg ~0.2‰ in the Zhijin and Tongren sections; Wu et al., 2022; Yin et al., 2017; Zhu et al., 2021a). Therefore, the wide range of δ^{202}Hg and Δ^{199}Hg values and low–middle Hg/TOC ratios (mostly < 150) in the lower part of all mentioned sections indicate that volcanic contributions could not play a significant role in widespread Hg enrichment in the Nanhua Basin.

Transmission of pelagic-seawater (in the open ocean) by subsurface paleocurrents has also been invoked to explain moderate Hg enrichment (Hg/TOC = 50–200) during the Cretaceous Oceanic Anoxic Events (OAE1a and OAE2; Scaife et al., 2017). It should be noted that the lowest parts of Shuijingtuo (Qinjiang core), Yu'anshan (Chengjiang core), and Niutitang Formations represent a large-scale transgression event (Jin et al., 2016), when the upwelling of a pelagic-seawater-enriched dissolved organic carbon (DOC) reservoir have generated negative carbonate and organic carbon δ^{13}C excursions (Jiang et al., 2012). The transgression event may have also transported large amounts of dissolved Hg associated with DOC (Hg-DOC) into the Nanhua Basin because dissolved Hg is usually bonded to DOC in pelagic seawater (Fitzgerald et al., 2007). The upwelling of a Hg-DOC-enriched reservoir and local precipitation of Hg associated with organic matter or sulfide in anoxic conditions would result in moderate Hg enrichment in local sediments. This mechanism has been proposed to explain Hg enrichment (Hg ~ 400–1000 ppb, Hg/TOC ~ 80) in anoxic marine sediments from the Nanhua Basin during the Ediacaran Shuram excursion (Fan et al., 2021). Furthermore, higher total Hg concentrations, more positive Δ^{199}Hg values, and more negative δ^{202}Hg values in the deeper shelf and slope shales (Zhijing and Tongren sections) than in the shallow water delta sediments (the lower part of Chengjiang core, this study) and, to a lesser extent, shallow shelf shales (the lower part of Qingjiang core, this study; Figs. 2–4) indicate the enriched Hg in these shales could be sourced from different endmember reservoirs. One endmember could be local/regional terrestrial plus atmospheric deposition. Another could be upwelling Hg-DOC associated with pelagic seawater in the open/global ocean, possibly characterized by mostly negative δ^{202}Hg (−2.08 ± 0.61 ‰) and positive Δ^{199}Hg (0.21 ± 0.06 ‰; Fig. 4; Štrok et al., 2015). This hypothesis is also supported by a negative correlation between δ^{13}C of organic carbon and Δ^{199}Hg values in the lower part of the Niutitang Formation in the Tongren region ($R^2 = 0.60$, $p < 0.01$; Wu et al., 2022), and it can easily explain elevated Hg (up to 1170 ppb) and TOC (mostly > 10%, up to 20%) in the lower Niutitang Formation deeper shelf and slope shales. However, Hg isotopes of the lowest parts of the Shuijingtuo (Qinjiang) and Yu'anshan (Chengjiang) Formations demonstrate lesser Hg-DOC contributions from the open ocean (Fig. 4). Another possibility is that Hg isotope signatures of Hg-DOC upwelling from pelagic ocean were overprinted by those of the local terrestrial and atmospheric Hg. In summary, Hg enrichment in the deeper shelf (Zhijin) and slope (Tongren) shales could be mainly attributed to Hg-DOC upwelling from the open ocean, but Hg in the shallow shelf shales (Qingjiang, this study) could be dominantly controlled by local atmospheric and possibly terrestrial inputs (Fig. 4).

5.2. Hg isotope excursions through the fossiliferous strata (~518 Ma)

Decreasing total Hg concentrations and negative Δ^{199}Hg excursions after the Hg-enrichment interval (i.e., through the fossiliferous strata,

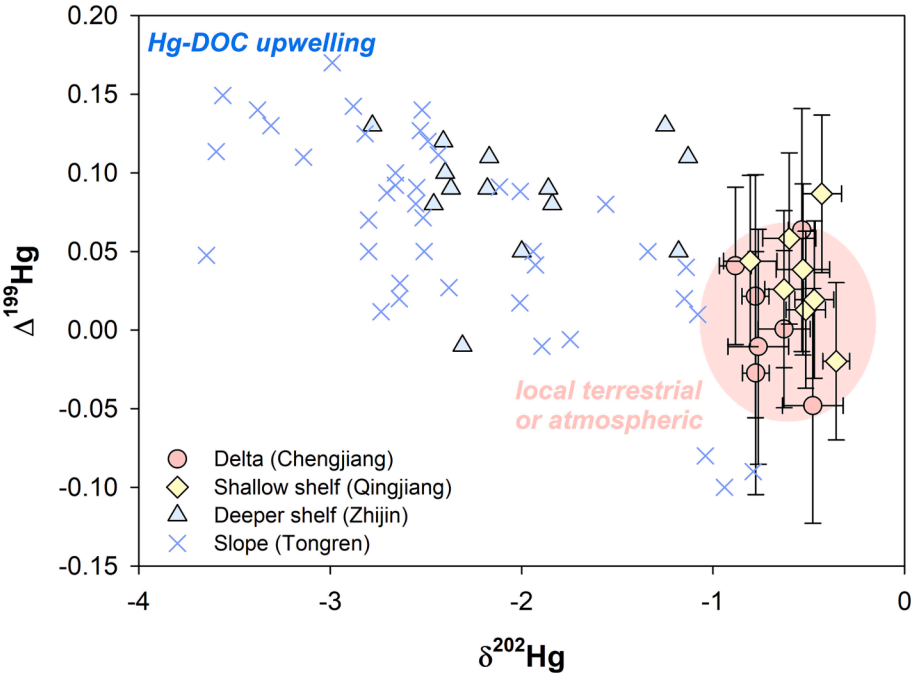

Fig. 4. Correlations of Δ^{199}Hg and δ^{202}Hg in Nanhua Basin shales. Relationships could indicate local atmospheric and/or terrestrial contributions in the shallow water locations during Hg-enrichment interval prior to the occurrence of Chengjiang and Qingjiang Biotas, as well as Hg associated with dissolved organic carbon (Hg-DOC) upwelling from the pelagic seawater to deeper shelf and slope regions. The Zhijin and Tongren sections are taken from refs. (Wu et al., 2022; Yin et al., 2017; Zhu et al., 2021a).

shaded blue in Fig. 2) are observed in our investigated cores (Fig. 2A and B). These trends may reflect a change of the dominant Hg source and/or the varying seawater redox conditions. For instance, declines of total Hg and Δ^{199}Hg (from 0.15 ‰ to −0.20 ‰) in the deeper shelf and slope sections from the Nanhua Basin (Fig. 2C) and the Indian Craton have been attributed to increasing terrestrial contributions (Liu et al., 2021b; Wu et al., 2022; Zhu et al., 2021a). As mentioned earlier, Hg sourced from terrestrial weathering during Precambrian time could be characterized by near-zero Δ^{199}Hg and less negative δ^{202}Hg (e.g., −0.6 ‰ to −0.1 ‰) signatures due to the paucity of land plants (Meixnerová et al., 2021). The fossiliferous strata in the Chengjiang core indeed correspond to a regression episode, when periodic freshwater discharge transports important terrestrial material into deltaic environments (Saleh et al., 2022). The up-section increase of δ^{202}Hg and negative or near-zero Δ^{199}Hg values in the Chengjiang core (depth of 15–51 m) may therefore indicate an increasing terrestrial contribution, which is compatible with deposition in a very nearshore delta environment (Saleh et al., 2022). However, the significant negative Δ^{199}Hg excursions to values <−0.1 ‰ observed in the more distal Qingjiang and slope Tongren sections (Fig. 2B and C; Wu et al., 2022; Zhu et al., 2021a) could not be caused by the enhanced terrestrial contributions alone.

The occurrence of Hg isotope excursions in both the Nanhua Basin (this study) and the Indian Craton (Liu et al., 2021b) may not be coincidental. Following existing chemical stratigraphic correlations (Li et al., 2021; Wu et al., 2022), these excursions could be mostly isochronous. In turn, these excursions indicate a significant regional and/or global change of Hg geochemical cycling could have taken place during this time. Modern oceanic Hg biogeochemical cycling studies (Jiskra et al., 2021; Shah et al., 2021) have demonstrated deposition of atmospheric Hg (0) and Hg (II) are the two major sources of Hg in the open ocean. The mean Δ^{199}Hg value of gaseous Hg (0) is approximately 0.50 ‰ lower than that of atmospheric Hg (II) in modern environments (Jiskra et al., 2021; Sun et al., 2019). Deposition of atmospheric Hg (0) in the ocean is mainly controlled by water–atmosphere bi-directional diffusion and subsequent photochemical, abiotic aphotic, and oxidation processes in surface waters, the latter of which could be greatly enhanced in oxygenated seawater containing H_2O_2, chloride, and Mn/Fe-oxides (Amyot et al., 2005; Lalonde et al., 2001; Siciliano et al., 2002; Zhang et al., 2015). In addition, two studies suggested that the negative shifts of Hg MIF in late Mesoproterozoic (~1.1 Ga) and Neoproterozoic (635–551 Ma) shales were most likely caused by the enhanced sequestration of atmospheric Hg (0) to sediments by thiols and sulfide that were enriched in the surface ocean due to photic zone euxinia (Zheng et al., 2018; Zheng et al., 2023). However, Fe species data indicated a contraction of euxinic conditions and TOC/P ratios and Mn concentrations suggest an expansion of oxic conditions in the Nanhua basin at that time (Li et al., 2021; this study). Therefore, we propose that increased uptake of atmospheric Hg (0) by surface seawater could be driven by enhanced oxidation of Hg (0) due to the transition from anoxic to oxic conditions. During this process, Hg (0) was strongly adsorbed on the MnO_2 surfaces via chemisorption mechanism and oxidized to Hg (I) and then Hg (II) (Zhang et al., 2015; Zhang et al., 2014). Given the negative Δ^{199}Hg signals of atmospheric Hg (0) and the subsequent negative Hg (II) odd-mass independent fractionation (odd-MIF) produced during oxidation processes (Zheng et al., 2019), enhanced adsorption of Hg (0) by Mn-oxides and conversion to Hg (II) and, finally, removal to marine sediments under oxidizing conditions is expected to contribute to the negative Δ^{199}Hg excursions recorded by fossiliferous strata. Total Hg concentrations remains at relatively low levels because the sequestration of atmospheric depositional Hg (II) by organic matter could have been strongly limited.

In addition to the precipitation pathways of atmospheric Hg (0), odd-MIF induced by photochemical reduction of Hg (II) species, under anoxic or oxic conditions, is also a potential trigger for changes in Δ^{199}Hg values. Previous experimental studies show that the photoreduction of Hg (II) complexed with S-donor ligands (Hg-SR) under neutral-pH anoxic conditions, Hg (II) complexed with O-donor ligands (Hg-OR), and methylmercury (MeHg) produce positive Δ^{199}Hg in residual dissolved Hg (II) pools, whereas photoreduction of Hg-SR under neutral pH oxic conditions and Hg (II) complexed with Cl (Hg (II)-Cl) produce negative Δ^{199}Hg in residual Hg pools (Bergquist and Blum, 2007; Motta et al., 2020; Zheng and Hintelmann, 2010). In anoxic seawater, Hg (II)-SR, Hg (II)-OR, and MeHg are the dominant Hg (II) species (Fitzgerald et al., 2007), and the photoreduction of these Hg (II) species produces positive odd-MIF in seawater (Bergquist and Blum, 2007; Motta et al., 2020; Zheng and Hintelmann, 2010). By contrast, photoreduction of the increased Hg (II)-Cl complexes and the relatively minor Hg (II)-SR complexes in neutral pH, oxic seawaters would generate negative odd-MIF (Fitzgerald et al., 2007; Motta et al., 2020), which is expected to offset or out-compete the positive odd-MIF generated by Hg (II)-OR complexes during photoreduction, leading to less positive or even negative Δ^{199}Hg in seawater.

As a benthic redox proxy, decreasing TOC/P values to <10–20 (TOC/P < 30 in fully oxic Amazon shelf and Blake Plateau sediments; Algeo and Ingall, 2007), together with increasing Mn concentrations, show a redox transition of both bottom and surface water from anoxic towards oxic conditions after the Hg enrichment interval in both the Chengjiang and Qinjiang cores (Fig. 2A and B). These trends are also consistent with the decreasing Mo and U concentrations recorded in other shelf and slope sections (Han et al., 2018; Li et al., 2021). Moreover, positive and negative correlations of Δ^{199}Hg values with TOC/P ratios and Mn concentrations, respectively, in the Qingjiang core (Fig. 5A, B) could indicate increasing oxygen levels in local seawater were an important factor controlling variations of Δ^{199}Hg values. This can be also evidenced by the same positive correlation between Δ^{199}Hg and TOC/P ratios recorded in the Chengjiang core ($R^2 = 0.40$, $p < 0.01$). However, the absence of a negative relationship between Δ^{199}Hg and Mn concentrations in the Chengjiang core, could be attributed to abundant terrestrial materials input (Mn-Al, $R^2 = 0.52$, $p < 0.01$). The higher concentrations of Mn-oxides (in the presence of Cl^-) may stimulate the adsorption and subsequently oxidation of Hg (0) to Hg (II) and removal into sediments (Zhang et al., 2015; Zhang et al., 2014), although this mechanism could not induce extra Hg MIF. During the transition from the anoxic period to the oxic period (evidenced by TOC/P ratios and Mn concentrations in this study and Fe species, S, and U isotope data reviewed by Li et al. (2021)), chemical effects of enhanced uptake of atmospheric Hg (0) by oxygenated seawater and photoreduction of major Hg (II)-Cl and minor Hg (II)-SR complexes would be greater than those of positive odd-MIF produced by photoreduction of Hg (II)-OR complexes, causing an observed negative shift of Δ^{199}Hg in the Nanhua Basin and the Indian Craton. Therefore, an appreciable (i.e., 0.15–0.3 ‰) negative Δ^{199}Hg shift could reflect a significant oxygenation event after Hg enrichment (i.e., during the deposition of fossiliferous strata), but the potential mechanism should be investigated further.

We further speculated that this oxygenation hypothesis is supported by a pronounced negative shift of δ^{202}Hg values observed in most offshore sediments from the Qingjiang (−0.53 ‰ to −2.74 ‰; Fig. 2B), Zhijin (−1.58 ‰ to −2.78 ‰) and Tongren (−2.55 ‰ to −4.03 ‰; Fig. 2C) sections during deposition of the fossiliferous strata (Yin et al., 2017; Zhu et al., 2021a). Although Hg MDF is complex and caused by different physical, chemical, and biological pathways (e.g., Blum et al., 2014; Grasby et al., 2019), clear correlations of δ^{202}Hg with TOC/P ratios ($R^2 = 0.58$, $p < 0.01$) and Mn concentrations ($R^2 = 0.50$, $p < 0.01$) are observed in the Qingjiang core (Fig. 5C, D). These observations could indicate Hg MDF is also controlled by seawater redox conditions, where the oxidation of Mn^{2+} and subsequent precipitation of Mn-oxides could preferentially adsorb isotopically light Hg, resulting in more negative δ^{202}Hg values preserved by more oxic sediments. However, an experimental study suggested a fractionation only up to approximately −0.4 ‰ during the adsorption of Hg (II) on Fe oxides (Jiskra et al., 2012), which may be insufficient to induce a negative excursion of −1.5 ‰ in the Qingjiang core. A recent study indicated that δ^{202}Hg can be altered

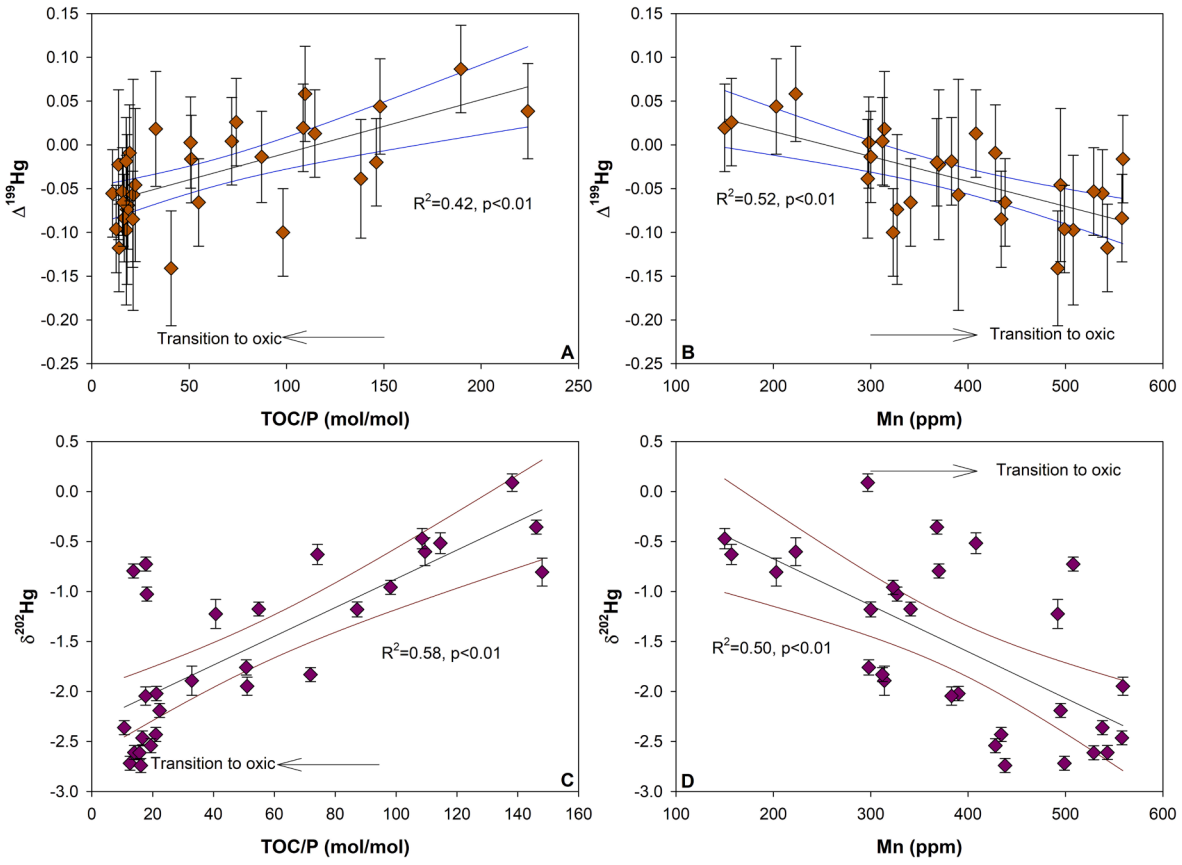

Fig. 5. Δ^{199}Hg and δ^{202}Hg plotted against TOC/P ratios and Mn concentrations in the Qingjiang core. The data indicate redox conditions of the seawater column have strongly controlled Hg isotopic variations. Three samples with abnormal relation between TOC/P ratios and Mn concentrations are not included.

(0.3–0.7 ‰) during the thermal maturation process, and the direction of change can be either positive or negative (Liu et al., 2022). Although the influence of the regional thermal maturation processes could not be excluded, it is likely that Hg MDF could be associated with the adsorption and oxidation of Hg (0) by Mn-oxides in the water column and the desorption and re-adsorption (or reduction and re-oxidation) at the water-sediments interface or in porewater. These processes have been invoked to explain the extremely large Se isotope fractionation (−12.77 ‰ to 4.93 ‰) at the chemocline (Wen and Carignan, 2011). The δ^{202}Hg values in the Chengjiang core do not show any correlation with TOC/P ratios and Mn concentrations (Fig. 2A), which may suggest that the influence of terrestrial contributions to Hg MDF overwhelmed that of redox conditions. Therefore, it is important to exercise caution when linking Hg MDF to redox variations. No Mn concentrations and TOC/P ratios were reported for the deeper water Zhijin and Tongren sections, but samples with the more negative δ^{202}Hg values usually show lower TOC concentrations in the Zhijin and Tongren sections, suggesting oxidation of abundant organic matter by Mn-oxides or free oxygen in the ancient water column. When this mechanism became the dominant fractionation pathway, it would disrupt the pre-existing shallow water Hg isotope fractionation system (atmosphere–ocean exchange layer), enhance adsorption and oxidation of Hg (0) and out-compete photoreduction of Hg (II), during which less positive and even negative Δ^{199}Hg could be preserved in most offshore sediments.

5.3. *Hg isotopes as a paleo-redox proxy of the Precambrian ocean and/or atmosphere*

Negative Δ^{199}Hg values in Precambrian marine sediments have been explained by the input of Hg via soil erosion (Deng et al., 2022a; Wu et al., 2022; Zhu et al., 2021a). However, terrestrial Hg before the evolution of land plants could not show obviously negative Δ^{199}Hg values like modern soil (e.g., Fan et al., 2021). Instead, the negative Δ^{199}Hg values could be mainly produced by Hg cycling in seawater and atmosphere, via the oxidation of Hg (0) by halogen compounds and/or H_2O_2 (Sun et al., 2022), and the enhanced sequestration of atmospheric Hg (0) to the sediments by thiols and sulfide (Zheng et al., 2018; Zheng et al., 2023). It is noteworthy that previous studies have reported four negative excursions of Δ^{199}Hg values during the Neoproterozoic, including at ~850–760 Ma (0 ‰ to −0.21 ‰), ~ 660–650 Ma (0 ‰ to −0.28 ‰), ~ 570 Ma (0.01 ‰ to −0.35 ‰), and ~518–510 Ma (0 ‰ to −0.18 ‰) (Deng et al., 2022b; Fan et al., 2021; Liu et al., 2021a; Sun et al., 2022). Among them, the negative Δ^{199}Hg values at ~660–650 Ma could be caused by oceanic and atmospheric oxygenation through the release of photochemically produced H_2O_2 in melting glaciers in the aftermath of the Sturtian glaciation, during that time abundant dissolved Fe was oxidized to form banded iron formation (Sun et al., 2022). The ~570 Ma negative Δ^{199}Hg values are also corresponding to a global oceanic oxygenation event during the Shuram carbon isotope excursion (Fan et al., 2021). The ~518–510 Ma negative Δ^{199}Hg values are associated with a local/global oceanic oxygenation event (This study). As discussed in Section 5.2, δ^{202}Hg values do not always show regular variations with redox proxies such as Mn concentrations and TOC/P ratios, which could be due to complex Hg MDF processes occurring in seawater and the atmosphere. However, most Δ^{199}Hg and δ^{202}Hg values during these oxygenation events do not show normal source-controlled negative correlations recorded in marine sediments. Therefore, we suggest that Hg isotopes are a promising potential paleo-redox proxy of the Precambrian ocean and/or atmosphere, but more further investigations are necessary.

5.4. Oceanic oxygenation stimulated Cambrian biodiversity development

In the Nanhua Basin, the occurrence of volcanic tuff at ~526 Ma in the Yunnan, Guizhou, and Hubei Provinces indicates significant volcanism (Compston et al., 2008; Okada et al., 2014). Extensive volcanism could release massive amounts of greenhouse and reducing gases (such as CO_2, H_2S, and Hg) into oceans, causing high surface water temperatures, ocean anoxia, and seawater acidification in shelf basins, all of which could destroy oceanic ecosystems and possibly cause the extinction of small shelly fauna in shallow waters, as well as localized, extreme Hg enrichment (Wang et al., 2020; Wu et al., 2022). Volcanic Hg input could also result in near zero Δ^{199}Hg and homogenous δ^{202}Hg signals (and extremely high Hg/TOC ratios) in relatively shallow water sediments, which are not displayed by the data from the Chengjiang and Qingjiang cores, nor the other deeper shelf and slope sections. However, it is important to consider that upwelling currents could transport Hg-DOC-rich water masses from pelagic seawater to clay-rich shallow seawater during transgressions, where clay sediments efficiently mix with Hg-DOC, causing large amounts of Hg-DOC to be adsorbed by clay sediments and preserved in deeper shelf and slope shales, such as the Zhijin, Tongren, and Jishou sections (Fig. 6A). This mechanism has been recently proposed as an alternative interpretation for the formation of organic-rich shales (Zhang, 2021), which would also stimulate and expand euxinic seawater conditions in the Nanhua Basin and the Indian Craton through a complex interaction between continental dissolved sulfate and upwelling DOC from the open ocean. The euxinic seawater would inherently facilitate Hg precipitation as sulfide and inhibit biological activity. As such, we argue (1) positive Δ^{199}Hg and more negative δ^{202}Hg signals in deeper shelf and slope sediments (Zhijin and Tongren sections) could be mostly due to Hg-DOC upwelling, and (2) high TOC concentrations (up to 20 %) recorded in most slope organic-rich shales from the lowest part of the Niutitang Formation (~521 Ma) may not be directly linked to locally elevated primary production, as proposed by previous studies (Cheng et al., 2020; Jin et al., 2016). This hypothesis is also supported by low δ^{114}Cd (~0.2 ‰) values in the deeper shelf Zhijin section and species richness of acritarchs, which are inconsistent with enhanced primary productivity during the Hg- and organic-enrichment interval (Frei et al., 2021; Li et al., 2021).

In the aftermath of volcanism and upwelling of the Hg-DOC reservoir (Fig. 6B), almost all redox sensitive trace elements (Mo, U, and V) and Hg show gradually decreasing concentrations in marine sediments of the Shuijingtuo, Yu'anshan, and Niutitang Formations. A possible cause of this is an oceanic oxygenation event during the late Cambrian Age 2 to middle of Cambrian Age 3 (Li et al., 2017; Li et al., 2021), which is also supported by decreasing TOC/P ratios and increasing Mn concentrations in the Chengjian and Qingjiang cores. The negative shifts of Δ^{199}Hg and δ^{202}Hg through the fossiliferous strata suggests enhanced adsorption and oxidation of Hg (0) by Mn-oxides (as well as significant photochemical reduction of Hg (II) in near-neutral, oxidizing shallow seawater and transport into deeper water sediments; Fig. 6B), indicating a significant oceanic oxygenation event occurred in the Nanhua Basin and the Indian Craton. Other redox proxy data (such as Mo and U isotopes) from elsewhere in the world (i.e., Oman, Tarim, and Siberia) suggest this oxygenation event could be a widespread, global period of oceanic oxygenation (reviewed in Wei et al., 2021). Nevertheless, this oxygenation episode is not only coupled to the diversification of the Chengjiang and Qingjiang Biotas in the Nanhua Basin, but it also coincides with a sharp increase in global biodiversity of marine

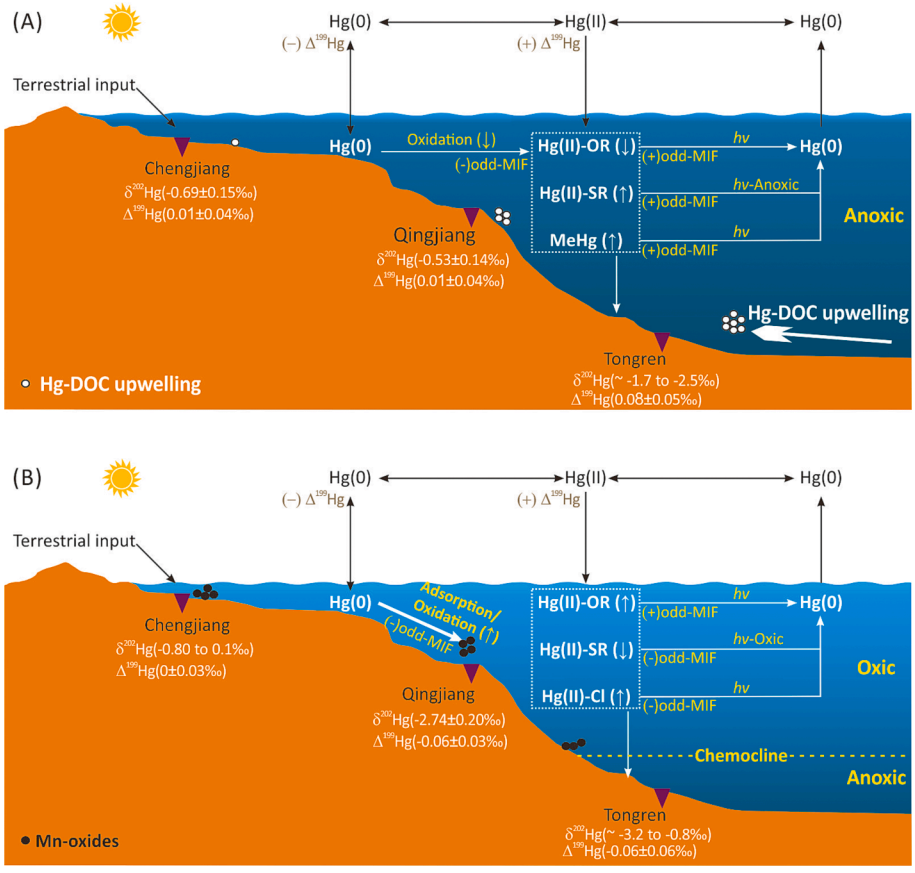

Fig. 6. (A) Hg geochemical cycling and fractionation of Hg isotopes in an anoxic seawater column before Cambrian radiation, accompanied by significant terrestrial input in shallow water shelf and Hg-DOC upwelling from the pelagic ocean in deeper shelf and slope locations, and (B) an oxidizing seawater column occurring during and slightly before deposition of the fossiliferous strata. (↑) and (↓) indicate that the processes and/or relative fractions of Hg (II) species in total Hg (II) are increasing and decreasing, respectively.

invertebrates during the Cambrian Age 3 (Na and Kiessling, 2015). Furthermore, a positive $\delta^{114}Cd$ shift of ~0.4 ‰ in the Niutitang Formation in one shelf Zhijin section also indicates high primary productivity (Frei et al., 2021). High primary productivity would also enhance free oxygen levels in the shallow shelf waters and provide sufficient food and energy for animals (Sperling and Stockey, 2018). However, the lower TOC could be caused by the strong degradation of organic matter in an oxic seawater and/or the dilution of enhanced regional terrestrial materials input. Finally, we argue that rising molecular oxygen in seawater, associated with enhanced marine primary productivity, may have been a critical driver of the Cambrian explosion.

6. Conclusions

In this contribution, we demonstrate the utility of coupled $\Delta^{199}Hg$ and $\delta^{202}Hg$ signals in marine sediments (where Hg is dominantly sourced from the atmosphere) as a seawater, and possibly atmospheric, paleoredox proxy, especially during periods before the evolution of land plants. Furthermore, we provide compelling evidence for a significant, large-scale, or even global oxygenation event during the summit of the Cambrian explosion. We also propose oxygenation of surface to deep seawater, induced by the enhanced primary productivity, may have facilitated the Cambrian explosion. Although the extent of global oxygenation during this time needs to be examined further, our data and interpretations add evidence and new details strengthening the mechanistic relationship between rising oxygen levels and the Cambrian explosion.

Declaration of Competing Interest

The authors declare that they have no known competing financial interests or personal relationships that could have appeared to influence the work reported in this paper.

Acknowledgments

This research was funded by the NSFC (41890841, U1812402, 42073016, 92062221, 42121003), the CAS (ZDBS-LY-DQC029) and the Guizhou Provincial 2020 Science and Technology Subsides (GZ2020SIG). We give thanks to Linhao Cui and Chao Chang for their assistance during sampling, to Yan'an Shen and Maoyan Zhu for improving manuscript and to editors and reviewers for their thoughtful and thorough reviews of our manuscript.

Appendix A. Supplementary material

The supplementary material includes Tables S1–S3, which provide Hg isotope data and other elemental concentrations (Hg, TOC, TS, Mn, P) from this study. Supplementary material to this article can be found online at https://doi.org/10.1016/j.gca.2023.10.020.

References

Algeo, T.J., Ingall, E., 2007. Sedimentary C_{org}: P ratios, paleocean ventilation, and Phanerozoic atmospheric p_O2. Palaeogeogr. Palaeoclimatol. Palaeoecol. 256, 130–155.
Amyot, M., Morel, F.M.M., Ariya, P.A., 2005. Dark oxidation of dissolved and liquid elemental mercury in aquatic environments. Environ. Sci. Technol. 39, 110–114.
Bergquist, B.A., Blum, J.D., 2007. Mass-dependent and -independent fractionation of Hg isotopes by photoreduction in aquatic systems. Science 318, 417–420.
Blum, J.D., Sherman, L.S., Johnson, M.W., 2014. Mercury isotopes in Earth and environmental sciences. Annu. Rev. Earth Planet. Sci. 42, 249–269.
Chang, C., Wang, Z., Huang, K.-J., Yun, H., Zhang, X., 2022. Nitrogen cycling during the peak Cambrian explosion. Geochim. Cosmochim. Acta 336, 50–61.
Cheng, M., Li, C., Jin, C., Wang, H., Algeo, T.J., Lyons, T.W., Zhang, F., Anbar, A., 2020. Evidence for high organic carbon export to the early Cambrian seafloor. Geochim. Cosmochim. Acta 287, 125–140.
Cloud, P.E., 1968. Atmospheric and hydrospheric evolution on the primitive earth. Both secular accretion and biological and geochemical processes have affected earth's volatile envelope. Science 160 (3829), 729–736.
Compston, W., Zhang, Z., Cooper, J.A., Ma, G., Jenkins, R.J.F., 2008. Further SHRIMP geochronology on the early Cambrian of South China. Am. J. Sci. 308, 399.
Deng, C., Geng, H., Xiao, T., Chen, D., Sun, G., Yin, R., 2022a. Mercury isotopic compositions of the Precambrian rocks and implications for tracing mercury cycling in Earth's interior. Precambr. Res. 373, 106646.
Deng, C., Zhang, J., Hu, R., Luo, K., Zhu, Y., Yin, R., 2022b. Mercury isotope constraints on the genesis of late Mesozoic Sb deposits in South China. Sci. China Earth Sci. 65, 269–281.
Erwin, D.H., Laflamme, M., Tweedt, S.M., Sperling, E.A., Pisani, D., Peterson, K.J., 2011. The Cambrian conundrum: early divergence and later ecological success in the early history of animals. Science 334, 1091–1097.
Fan, H., Fu, X., Ward, J.F., Yin, R., Wen, H., Feng, X., 2021. Mercury isotopes track the cause of carbon perturbations in the Ediacaran ocean. Geology 49, 248–252.
Fitzgerald, W.F., Lamborg, C.H., Hammerschmidt, C.R., 2007. Marine biogeochemical cycling of Mercury. Chem. Rev. 107, 641–662.
Frei, R., Xu, L., Frederiksen, J.A., Lehmann, B., 2021. Signals of combined chromium–cadmium isotopes in basin waters of the Early Cambrian – Results from the Maoshi and Zhijin sections, Yangtze Platform, South China. Chem. Geol. 563, 120061.
Fu, D., Tong, G., Dai, T., Liu, W., Yang, Y., Zhang, Y., Cui, L., Li, L., Yun, H., Wu, Y., Sun, A., Liu, C., Pei, W., Gaines, R.R., Zhang, X., 2019a. The Qingjiang biota-A Burgess Shale-type fossil Lagerstatte from the early Cambrian of South China. Science 363, 1338–1342.
Fu, X., Zhang, H., Liu, C., Zhang, H., Lin, C.-J., Feng, X., 2019b. Significant seasonal variations in isotopic composition of atmospheric total gaseous Mercury at forest sites in china caused by vegetation and Mercury sources. Environ. Sci. Technol. 53, 13748–13756.
Gehrke, G.E., Blum, J.D., Meyers, P.A., 2009. The geochemical behavior and isotopic composition of Hg in a mid-Pleistocene western Mediterranean sapropel. Geochim. Cosmochim. Acta 73, 1651–1665.
Grasby, S.E., Shen, W., Yin, R., Gleason, J.D., Blum, J.D., Lepak, R.F., Hurley, J.P., Beauchamp, B., 2017. Isotopic signatures of mercury contamination in latest Permian oceans. Geology 45, 55–58.
Grasby, S.E., Them, T.R., Chen, Z., Yin, R., Ardakani, O.H., 2019. Mercury as a proxy for volcanic emissions in the geologic record. Earth Sci. Rev. 196, 102880.
Hammarlund, E.U., Gaines, R.R., Prokopenko, M.G., Qi, C., Hou, X.-G., Canfield, D.E., 2017. Early Cambrian oxygen minimum zone-like conditions at Chengjiang. Earth Planet. Sci. Lett. 475, 160–168.
Hammarlund, E.U., von Stedingk, K., Påhlman, S., 2018. Refined control of cell stemness allowed animal evolution in the oxic realm. Nat. Ecol. Evol. 2, 220–228.
Hammarlund, E.U., Smith, M.P., Rasmussen, J.A., Nielsen, A.T., Canfield, D.E., Harper, D.A.T., 2019. The Sirius Passet Lagerstätte of North Greenland—A geochemical window on early Cambrian low-oxygen environments and ecosystems. Geobiology 17, 12–26.
Han, T., Fan, H., Wen, H., 2018. Dwindling vanadium in seawater during the early Cambrian, South China. Chem. Geol. 492, 20–29.
Jiang, G., Wang, X., Shi, X., Xiao, S., Zhang, S., Dong, J., 2012. The origin of decoupled carbonate and organic carbon isotope signatures in the early Cambrian (ca. 542–520Ma) Yangtze platform. Earth Planet. Sci. Lett. 317–318, 96–110.
Jin, C., Li, C., Algeo, T.J., Planavsky, N.J., Cui, H., Yang, X., Zhao, Y., Zhang, X., Xie, S., 2016. A highly redox-heterogeneous ocean in South China during the early Cambrian (~529–514 Ma): Implications for biota-environment co-evolution. Earth Planet. Sci. Lett. 441, 38–51.
Jiskra, M., Wiederhold, J.G., Bourdon, B., Kretzschmar, R., 2012. Solution speciation controls mercury isotope fractionation of Hg(II) sorption to goethite. Environ. Sci. Technol. 46, 6654–6662.
Jiskra, M., Heimburger-Boavida, L.E., Desgranges, M.M., Petrova, M.V., Dufour, A., Ferreira-Araujo, B., Masbou, J., Chmeleff, J., Thyssen, M., Point, D., Sonke, J.E., 2021. Mercury stable isotopes constrain atmospheric sources to the ocean. Nature 597, 678–682.
Knoll, A.H., Carroll, S.B., 1999. Early animal evolution: Emerging views from comparative biology and geology. Science 284, 2129.
Lalonde, J.D., Amyot, M., Kraepiel, A.M.L., Morel, F.M.M., 2001. Photooxidation of Hg (0) in artificial and natural waters. Environ. Sci. Technol. 35, 1367–1372.
Lehmann, B., Näg̈ler, T.F., Holland, H.D., Wille, M., Mao, J., Pan, J., Ma, D., Dulski, P., 2007. Highly metalliferous carbonaceous shale and Early Cambrian seawater. Geology 35, 403–406.
Lenton Timothy, M., Dahl Tais, W., Daines Stuart, J., Mills Benjamin, J.W., Ozaki, K., Saltzman Matthew, R., Porada, P., 2016. Earliest land plants created modern levels of atmospheric oxygen. PNAS 113, 9704–9709.
Li, C., Jin, C., Planavsky, N.J., Algeo, T.J., Cheng, M., Yang, X., Zhao, Y., Xie, S., 2017. Coupled oceanic oxygenation and metazoan diversification during the early–middle Cambrian? Geology, G39208.39201.
Li, Z., Zhang, M., Chen, Z.-Q., Algeo, T.J., Zhao, L., Zhang, F., 2021. Early Cambrian oceanic oxygenation and evolution of early animals: A critical review from the South China Craton. Global Planet. Change 204, 103561.
Liu, Z., Tian, H., Yin, R., Chen, D., Gai, H., 2022. Mercury loss and isotope fractionation during thermal maturation of organic-rich mudrocks. Chem. Geol. 612, 121144.
Liu, Z.-R.-R., Zhou, M.-F., Chen, W.T., Williams-Jones, A.E., Li, X.-D., Yin, R.-S., O'Brien, H., Lahaye, Y., 2021a. Mercury and sulfur isotopic evidence for the linkages between the ca. 510 Ma Kalkarindji large igneous province and trilobite crisis. Earth Planet. Sci. Lett. 566, 116947.
Liu, Z.-R.-R., Zhou, M.-F., Wang, W., 2021b. Mercury anomalies across the Ediacaran-Cambrian boundary: Evidence for a causal link between continental erosion and biological evolution. Geochim. Cosmochim. Acta 304, 327–346.

Mazrui, N.M., Jonsson, S., Thota, S., Zhao, J., Mason, R.P., 2016. Enhanced availability of mercury bound to dissolved organic matter for methylation in marine sediments. Geochim. Cosmochim. Acta 194, 153–162.
Meixnerová, J., Blum Joel, D., Johnson Marcus, W., Stüeken Eva, E., Kipp Michael, A., Anbar Ariel, D., Buick, R., 2021. Mercury abundance and isotopic composition indicate subaerial volcanism prior to the end-Archean "whiff" of oxygen. Proc. Natl. Acad. Sci. U.S.A. 118, e2107511118.
Mills, D.B., Canfield, D.E., 2014. Oxygen and animal evolution: Did a rise of atmospheric oxygen "trigger" the origin of animals? Bioessays 36, 1145–1155.
Motta, L.C., Kritee, K., Blum, J.D., Tsz-Ki Tsui, M., Reinfelder, J.R., 2020. Mercury isotope fractionation during the photochemical reduction of Hg(II) coordinated with organic ligands. Chem. A Eur. J. 124, 2842–2853.
Na, L., Kiessling, W., 2015. Diversity partitioning during the Cambrian radiation. PNAS 112, 4702–4706.
Okada, Y., Sawaki, Y., Komiya, T., Hirata, T., Takahata, N., Sano, Y., Han, J., Maruyama, S., 2014. New chronological constraints for Cryogenian to Cambrian rocks in the Three Gorges, Weng'an and Chengjiang areas. South China. Gondwana Res. 25, 1027–1044.
Paterson John, R., Edgecombe Gregory, D., Lee Michael, S.Y., 2019. Trilobite evolutionary rates constrain the duration of the Cambrian explosion. PNAS 116, 4394–4399.
Qi, C., Li, C., Gabbott, S.E., Ma, X., Xie, L., Deng, W., Jin, C., Hou, X.-G., 2018. Influence of redox conditions on animal distribution and soft-bodied fossil preservation of the Lower Cambrian Chengjiang Biota. Palaeogeogr. Palaeoclimatol. Palaeoecol. 507, 180–187.
Saleh, F., Qi, C., Buatois, L.A., Mángano, M.G., Paz, M., Vaucher, R., Zheng, Q., Hou, X.-G., Gabbott, S.E., Ma, X., 2022. The Chengjiang Biota inhabited a deltaic environment. Nat. Commun. 13, 1569.
Scaife, J.D., Ruhl, M., Dickson, A.J., Mather, T.A., Jenkyns, H.C., Percival, L.M.E., Hesselbo, S.P., Cartwright, J., Eldrett, J.S., Bergman, S.C., Minisini, D., 2017. Sedimentary Mercury enrichments as a marker for submarine large igneous province volcanism? Evidence from the mid-Cenomanian event and oceanic anoxic event 2 (Late Cretaceous). Geochem. Geophys. Geosyst. 18, 4253–4275.
Selin, N.E., 2009. Global biogeochemical cycling of Mercury: A review. Annu. Rev. Env. Resour. 34, 43–63.
Shah, V., Jacob, D.J., Thackray, C.P., Wang, X., Sunderland, E.M., Dibble, T.S., Saiz-Lopez, A., Cernusak, I., Kello, V., Castro, P.J., Wu, R., Wang, C., 2021. Improved mechanistic model of the atmospheric redox chemistry of Mercury. Environ. Sci. Technol. 55, 14445–14456.
Shen, J., Algeo, T.J., Chen, J., Planavsky, N.J., Feng, Q., Yu, J., Liu, J., 2019. Mercury in marine Ordovician/Silurian boundary sections of South China is sulfide-hosted and non-volcanic in origin. Earth Planet. Sci. Lett. 511, 130–140.
Shen, J., Feng, Q., Algeo, T.J., Liu, J., Zhou, C., Wei, W., Liu, J., Them, T.R., Gill, B.C., Chen, J., 2020. Sedimentary host phases of mercury (Hg) and implications for use of Hg as a volcanic proxy. Earth Planet. Sci. Lett. 543, 116333.
Siciliano, S.D., O'Driscoll, N.J., Lean, D.R.S., 2002. Microbial reduction and oxidation of Mercury in freshwater lakes. Environ. Sci. Technol. 36, 3064–3068.
Smith, C.N., Kesler, S.E., Blum, J.D., Rytuba, J.J., 2008. Isotope geochemistry of mercury in source rocks, mineral deposits and spring deposits of the California Coast Ranges, USA. Earth Planet. Sci. Lett. 269, 399–407.
Sperling, E.A., Frieder, C.A., Raman, A.V., Girguis, P.R., Levin, L.A., Knoll, A.H., 2013. Oxygen, ecology, and the Cambrian radiation of animals. PNAS 110, 13446.
Sperling, E.A., Stockey, R.G., 2018. The temporal and environmental context of early animal evolution: Considering all the ingredients of an "Explosion". Integr. Comp. Biol. 58, 605–622.
Sperling, E.A., Wolock, C.J., Morgan, A.S., Gill, B.C., Kunzmann, M., Halverson, G.P., Macdonald, F.A., Knoll, A.H., Johnston, D.T., 2015. Statistical analysis of iron geochemical data suggests limited late Proterozoic oxygenation. Nature 523, 451–454.
Štrok, M., Baya, P.A., Hintelmann, H., 2015. The mercury isotope composition of Arctic coastal seawater. C.R. Geosci. 347, 368–376.
Sun, R.Y., Enrico, M., Heimburger, L.E., Scott, C., Sonke, J.E., 2013. A double-stage tube furnace-acid-trapping protocol for the pre-concentration of mercury from solid samples for isotopic analysis. Anal. Bioanal. Chem. 405, 6771–6781.
Sun, R., Jiskra, M., Amos, H.M., Zhang, Y., Sunderland, E.M., Sonke, J.E., 2019. Modelling the mercury stable isotope distribution of Earth surface reservoirs: Implications for global Hg cycling. Geochim. Cosmochim. Acta 246, 156–173.
Sun, R., Grasby, S.E., Shen, J., Xiao, J., Yin, R., 2022. Climate/ocean dynamics and possible atmospheric mercury depletion events during the Late Sturtian deglaciation. Chem. Geol. 598, 120830.
Wang, Z., Tan, J., Boyle, R., Wang, W., Kang, X., Dick, J., Lyu, Q., 2020. Mercury anomalies within the lower Cambrian (stage 2–3) in South China: Links between volcanic events and paleoecology. Palaeogeogr. Palaeoclimatol. Palaeoecol. 558, 109956.
Wei, G.-Y., Planavsky, N.J., He, T., Zhang, F., Stockey, R.G., Cole, D.B., Lin, Y.-B., Ling, H.-F., 2021. Global marine redox evolution from the late Neoproterozoic to the early Paleozoic constrained by the integration of Mo and U isotope records. Earth Sci. Rev. 214, 103506.
Wen, H., Carignan, J., 2011. Selenium isotopes trace the source and redox processes in the black shale-hosted Se-rich deposits in China. Geochim. Cosmochim. Acta 75, 1411–1427.
Wu, Y., Yin, R., Li, C., Chen, D., Grasby, S.E., Li, T., Ji, S., Tian, H., Peng, P.A., 2022. Global Hg cycle over Ediacaran-Cambrian transition and its implications for environmental and biological evolution. Earth Planet. Sci. Lett. 587, 117551.
Xu, L., Bernd, L., Mao, J., Qu, W., Du, A., 2011. Re-Os age of polymetallic Ni-Mo-PGE-Au mineralization in early Cambrian Black Shales of South China—A reassessment. Econ. Geol. 106, 511–522.
Yang, C., Li, X.-H., Zhu, M., Condon, D.J., Chen, J., 2018. Geochronological constraint on the Cambrian Chengjiang biota, South China. J. Geol. Soc. (London, U.K.) 175, 659–666.
Yin, R., Xu, L., Lehmann, B., Lepak, R.F., Hurley, J.P., Mao, J., Feng, X., Hu, R., 2017. Anomalous mercury enrichment in Early Cambrian black shales of South China: Mercury isotopes indicate a seawater source. Chem. Geol. 467, 159–167.
Zerkle, A.L., Yin, R., Chen, C., Li, X., Izon, G.J., Grasby, S.E., 2020. Anomalous fractionation of mercury isotopes in the Late Archean atmosphere. Nat. Commun. 11, 1709.
Zhang, X., 2021. Marine refractory dissolved organic carbon and transgressive black shales. Chin. Sci. Bull. 67, 1607–1613.
Zhang, B., Liu, J., Zheng, C., Chang, M., 2014. Theoretical study of mercury species adsorption mechanism on MnO_2(110) surface. Chem. Eng. J. 256, 93–100.
Zhang, B., Liu, J., Yang, Y., Chang, M., 2015. Oxidation mechanism of elemental mercury by HCl over MnO_2 catalyst: Insights from first principles. Chem. Eng. J. 280, 354–362.
Zhang, X., Shu, D., 2021. Current understanding on the Cambrian Explosion: questions and answers. PalZ 95, 641–660.
Zheng, W., Gilleaudeau, G.J., Kah, L.C., Anbar, A.D., 2018. Mercury isotope signatures record photic zone euxinia in the Mesoproterozoic ocean. PNAS 115, 10594–10599.
Zheng, W., Demers, J.D., Lu, X., Bergquist, B.A., Anbar, A.D., Blum, J.D., Gu, B., 2019. Mercury stable isotope fractionation during abiotic dark oxidation in the presence of thiols and natural organic matter. Environ. Sci. Technol. 53, 1853–1862.
Zheng, W., Hintelmann, H., 2010. Isotope fractionation of mercury during its photochemical reduction by low-molecular-weight organic compounds. Chem. A Eur. J. 114, 4246–4253.
Zheng, W., Zhou, A., Sahoo, S.K., Nolan, M.R., Ostrander, C.M., Sun, R., Anbar, A.D., Xiao, S., Chen, J., 2023. Recurrent photic zone euxinia limited ocean oxygenation and animal evolution during the Ediacaran. Nat. Commun. 14, 3920.
Zhu, G., Wang, P., Li, T., Zhao, K., Zheng, W., Feng, X., Shen, J., Grasby, S.E., Sun, G., Tang, S., Yan, H., 2021a. Mercury record of intense hydrothermal activity during the early Cambrian, South China. Palaeogeogr. Palaeoclimatol. Palaeoecol. 568, 110294.
Zhu, M.Y., Zhang, J.M., Li, G.X., 2001. Sedimentary environments of the Early Cambrian Chengjiang Biota: Sedimentology of the Yu'anshan Formation in Chengjiang County, Eastern Yunnan. Acta Palaeontol. Sin. 40, 80–105.
Zhu, G., Zhao, K., Li, T., Zhang, Z., Tang, S., Wang, P., 2021b. Anomalously high enrichment of mercury in early Cambrian black shales in South China. J. Asian Earth Sci. 216, 104794.